ISSN 1070-3284, Russian Journal of Coordination Chemistry, 2014, Vol. 40, No. 12, pp. 875–884. © Pleiades Publishing, Ltd., 2014.
Original Russian Text © A.V. Ivanov, T.A. Rodina, O.V. Loseva, 2014, published in Koordinatsionnaya Khimiya, 2014, Vol. 40, No. 12, pp. 707–716.

Polymeric Complexes $([Au\{S_2CN(CH_2)_4O\}_2]_2[ZnCl_4] \cdot 2H_2O)_n$ and $([Au\{S_2CN(CH_2)_4O\}_2]Cl \cdot 2H_2O)_n$ as Individual Gold(III)-Binding Forms in the $[Zn_2\{S_2CN(CH_2)_4O\}_4]_n$–$[AuCl_4]^-$/2M HCl Chemisorption System: Supramolecular Self-Organization and Thermal Behavior

A. V. Ivanov[a, *], T. A. Rodina[b], and O. V. Loseva[a]

[a] *Institute of Geology and Nature Management, Far East Branch, Russian Academy of Sciences, Blagoveshchensk, Amur region, 675000 Russia*

[b] *Amur State University, Blagoveshchensk, Amur region, 675027 Russia*

**e-mail: alexander.v.ivanov@chemist.com*

Received May 13, 2014

Abstract—For freshly precipitated zinc complex with cyclic morpholinedithiocarbamate (MfDtc) ligand, the ability to extract gold(III) from solutions in 2 M HCl was studied. The hydrated ionic type polymeric complexes, $([Au\{S_2CN(CH_2)_4O\}_2]_2[ZnCl_4] \cdot 2H_2O)_n$ (**I**) and $([Au\{S_2CN(CH_2)_4O\}_2]Cl \cdot 2H_2O)_n$ (**II**), were preparatively isolated as individual gold-binding forms. The molecular and supramolecular structures of compounds **I** and **II** were established from single-crystal X-ray diffraction data; the thermal behavior was studied by simultaneous thermal analysis (STA). The structures of both compounds contain polymeric chains formed by the complex cations $[Au\{S_2CN(CH_2)_4O\}_2]^+$ through secondary non-valence Au···S bonds. The anionic part of the complexes is presented by structurally disordered tetrahedral $[ZnCl_4]^{2-}$ ions (in **I**) and polymeric chains involving water molecules and Cl^- anions (in **II**). The multistage thermal decomposition process comprises dehydration of the complexes, thermolysis of the cationic and anionic moieties with gold(III) reduction to the metal, release of zinc chloride, and partial formation of ZnS.

DOI: 10.1134/S1070328414120069

INTRODUCTION

The interest in dialkyldithiocarbamate zinc complexes (their synthesis, structure, and physicochemical properties) is largely caused by the applicability of these compounds for one-step preparation processes of nano-sized powders and film zinc sulfides (or heterometallic sulfides) with semiconductor properties [1–10]. In addition, zinc dithiocarbamate complexes with dialkyl-substituted ligands are capable of effective chemisorption of gold(III) from acidic solutions to give polynuclear and heteropolynuclear compounds with intricate supramolecular structures [11, 12]. Previously, in a study of the reaction of cadmium morpholinedithiocarbamate with solutions of $AuCl_3$, two individual gold(III)-binding forms were preparatively isolated, namely, the polymeric gold(III)–cadmium complex, $([Au\{S_2CN(CH_2)_4O\}_2]_2[CdCl_4] \cdot H_2O)_n$ [13], and an ionic gold(III) complex, $[Au_3\{S_2CN(CH_2)_4O\}_6][Au_2Cl_8][AuCl_4]$ [14].

In this study dealing with the reaction of zinc morpholinedithiocarbamate, $[Zn_2\{S_2CN(CH_2)_4O\}_4]$ (incorporating ligands with the cyclic structural fragment, $-N(CH_2)_4O$) with $[AuCl_4]^-$ in a 2M HCl solution, the hydrated complexes $[Au\{S_2CN(CH_2)_4O\}_2]_2[ZnCl_4] \cdot 2H_2O$ (**I**) and $[Au\{S_2CN(CH_2)_4O\}_2]Cl \cdot 2H_2O$ (**II**) were prepared and characterized in detail by X-ray diffraction, ^{13}C MAS NMR, and STA.

EXPERIMENTAL

Sodium morpholinedithiocarbamate (MfDtc) was prepared by the reaction of carbon disulfide (Merck) and morpholine (Aldrich) in alkaline medium [15], while the initial zinc complex [16] was obtained by precipitation of Zn^{2+} ions from the aqueous phase with NaMfDtc taken in stoichiometric ratio. The initial salt and zinc morpholinedithiocarbamate were characterized by ^{13}C MAS NMR spectroscopy (δ, ppm):

$Na\{S_2CN(CH_2)_4O\} \cdot 2H_2O$ (1 : 2 : 2): 204.8 ($-S_2CN=$); 67.6, 67.2 ($-OCH_2-$); 54.6, 53.9, 53.5 ($=NCH_2-$).

$[Zn_2\{S_2CN(CH_2)_4O\}_4]$: 200.4 (61)*, 199.7 (60)* (1 : 1, $-S_2CN=$); 67.4, 67.1 (1 : 3, $-OCH_2-$); 54.3, 53.6, 52.8, 50.8 (1 : 1 : 1 : 1, $=NCH_2-$).

(* Asymmetric $^{13}C-^{14}N$ doublets [17, 18], Hz.)

Synthesis of I and II. Bis(morpholinedithiocarbamato-S,S')gold(III) tetrachlorozincate (**I**) and

bis(morpholinedithiocarbamato-S,S')gold(III) chloride (**II**) were prepared by the reaction of the zinc complex freshly precipitated by MfDtc with a solution of $AuCl_3$ in 2M HCl. The heterogeneous reaction occurring by the chemisorption mechanism and including ion exchange can be written as follows:

$$2[Zn_2\{S_2CN(CH_2)_4O\}_4] + 4H[AuCl_4] = [Au\{S_2CN(CH_2)_4O\}_2]_2[ZnCl_4] + 2[Au\{S_2CN(CH_2)_4O\}_2]Cl + 3ZnCl_2 + 4HCl.$$

A solution of $AuCl_3$ (10 mL in 2 M hydrochloric acid) containing 45.3 mg of gold was added to zinc morpholinedithiocarbamate (100 mg) and the mixture was stirred for 1.5 h. (The residual content of gold in the solution was determined on a first-class 180–50 Hitachi atomic absorption spectrometer.) The resulting yellow precipitate was filtered off, washed with water, dried on the filter, and dissolved, with moderate heating, in an acetone–methanol mixture (1 : 1). For X-ray diffraction experiment, the crystals of polymeric complexes **I** (transparent yellow needle crystals) and **II** (prismatic crystals) were formed in hydrated modifications upon slow evaporation of the solvent.

^{13}C MAS NMR for **II**: 196.7, 195.2, 194.6 (2 : 1 : 1, $-S_2CN=$); 67.4, 66.9, 65.3 (2 : 3 : 3, $-OCH_2-$); 50.4, 49.7, 49.0, 48.4 ppm (4 : 2 : 1 : 1, $=NCH_2-$). (For compound **I**, a satisfactory MAS ^{13}C NMR could not be recorded.)

^{13}C MAS NMR spectra were recorded on a CMX-360 spectrometer (Agilent/Varian/Chemagnetics InfinityPlus) operating at 90.52 MHz, with a superconducting magnet with B_0 = 8.46 T and Fourier transformation. Proton cross-polarization was used and $^{13}C-^{1}H$ decoupling was used at a radiofrequency field on the proton resonance frequency [19]. Samples weighing ~50–100 mg were placed into a 4.0 mm ZrO_2 ceramic rotor. The magic angle spinning for recording the MAS ^{13}C NMR spectra was at 4600–5100(1) Hz; the acquisition number was 1200–13000; the $\pi/2$ proton pulses were 4.9 μs long; the $^{1}H-^{13}C$ contact time was 2.5 ms; and the pulse delay was 3.0 s. The isotropic ^{13}C chemical shifts (δ) are referred to the least shielded component of crystalline adamantane used as the external standard: δ= 38.48 ppm relative to tetramethylsilane.

X-ray diffraction analysis was performed on a Bruker-Nonius X8 Apex CCD diffractometer (MoK_α-radiation, λ = 0.71073 Å, graphite monochromator) at 150(2) K. The data were collected by a standard procedure: φ and ω scanning of narrow frames. The absorption corrections were applied empirically using the SADABS program package [20]. The structure was solved by the direct method and refined by the least squares method (on F^2) in the full-matrix anisotropic approximation for non-hydrogen atoms. The hydrogen atom positions were calculated geometrically and included in the refinement in the riding model. The data collection and editing and refinement of unit cell parameters were performed by the APEX2 [20] and SAINT [20] program packages. The structure solution and refinement were done using the SHELXTL program package [20]. The oxygen atoms of the hydrate molecules in compound **I** were found to be statistically disordered between two positions with equal occupancies (0.50), while the hydrogen positions in H_2O were not located. In compound **II**, the hydrogen atoms of the solvate water molecules were located in difference electron density syntheses and refined in the isotropic approximation with $U_{iso}(H) = 1.5U_{eq}(O)$ with the O–H distances of 0.89(2) and the H···H distances of 1.40(2) Å. Selected crystal data and structure refinement details for **I** and **II** are given in Table 1, bond lengths and bond angles are in Table 2, and the geometric parameters of hydrogen bonds are in Table 3.

The atom coordinates, bond lengths, and bond angles are deposited at the Cambridge Crystallographic Data Centre (nos. 995968 (**I**) and 995969 (**II**); deposit@ccdc.cam.ac.uk or http://www.ccdc.cam.ac.uk).

The thermal properties of I and II were studied by STA comprising simultaneous recording of thermogravimetric (TG) curves and differential scanning calorimetry (DSC). The measurements were performed on an STA 449C Jupiter instrument (NETZSCH) in corundum crucibles covered with a lid having a hole to maintain a vapor pressure of 1 atm during the thermal decomposition. The heating rate was 5°C/min up to 1100°C under an argon atmosphere. The sample weight was 1.829–2.984 mg. The accuracy of temperature measurement was ±0.7°C and the accuracy of measurement of mass changes was $\pm 1 \times 10^{-4}$ mg.

RESULTS AND DISCUSSION

The reaction of the starting complex $[Zn_2\{S_2CN(CH_2)_4O\}_4]$ with a solution of $AuCl_3$ was accompanied by fast reformation of the sorbent precipitate with change in its color from white to lemon yellow, indicating the formation of new compounds in the system. In parallel, the working solution decolorized. The degree of gold recovery from the solution was 98.7%.

The ^{13}C MAS NMR spectrum of compound **II** (Fig. 1) contains multicomponent groups of signals in the regions of $=NC(S)S-$, $-OCH_2-$, and $=NCH_2-$ (see Synthesis). The δ(^{13}C) values of dithiocarbamate groups in **II** are much smaller than in the starting zinc complex, which is attributable to residistribution of the MfDtc ligands into the inner sphere of gold. Due to the "heavy atom effect," the electronic system of gold is involved more efficiently in the additional shielding of the carbon atoms of the $=NC(S)S-$ groups. Fragment-by-fragment mathematical simulation of the spectra gave more accurate integrated intensity ratios for the ^{13}C signals from four (2 : 1 : 1) structurally non-equivalent $=NC(S)S-$ groups, eight $-OCH_2-$ groups (2 : 3 : 3), and eight $=NCH_2-$ groups (4 : 2 : 1 : 1). All this attests to an intricate structural

Table 1. Crystal data, X-ray experiment and structure refinement details for $[Au\{S_2CN(CH_2)_4O\}_2]_2[ZnCl_4] \cdot 2H_2O$ (**I**) and $[Au\{S_2CN(CH_2)_4O\}_2]Cl \cdot 2H_2O$ (**II**)

Parameter	Value	
Molecular formula	$C_{20}H_{36}N_4O_6S_8Cl_4Au_2Zn$	$C_{10}H_{20}N_2O_4S_4ClAu$
M	1286.11	592.94
System	Tetragonal	Monoclinic
Space group	$I4_1/a$	$P2_1/c$
a, Å	28.8000(12)	15.3426(10)
b, Å		15.6414(10)
c, Å	4.4205(2)	16.2689(12)
β, deg		109.586(2)
V, Å^3	3666.5(3)	3678.3(4)
Z	4	8
ρ_{calcd}, g/cm^3	2.330	2.141
μ, mm^{-1}	9.421	8.613
F(000)	2464	2288
Crystal size, mm	0.18 × 0.07 × 0.05	0.20 × 0.04 × 0.04
Data collection range of θ, deg	2.00–27.77	1.41–27.55
Ranges of reflection indices	$-35 \le h \le 37$, $-37 \le k \le 27$, $-5 \le l \le 1$	$-9 \le h \le 19$, $-20 \le k \le 14$, $-21 \le l \le 20$
The number of measured reflections	5756	13134
The number of independent reflections (R_{int})	2157 (0.0393)	8379 (0.0472)
Reflections with $I > 2\sigma(I)$	1791	5591
The number of refinement parameters	114	424
GOOF	1.095	0.929
R-factors for $F^2 > 2\sigma(F^2)$	$R_1 = 0.0483$, $wR_2 = 0.1291$	$R_1 = 0.0477$, $wR_2 = 0.0864$
R-factors for all reflections	$R_1 = 0.0595$, $wR_2 = 0.1341$	$R_1 = 0.0900$, $wR_2 = 0.0960$
Residual electron density (min/max), e Å^{-3}	−5.528/2.355	−1.892/2.270

Table 2. Selected bond lengths (*d*) and bond (ω) and torsion (φ) angles in structures **I** and **II***

Compound **I**			
Bond	*d*, Å	Bond	*d*, Å
Au(1)–S(1)	2.336(2)	N(1)–C(5)	1.475(12)
Au(1)–S(2)	2.340(2)	O(1)–C(3)	1.431(13)
Au(1)···S(1)[b]	3.663(2)	O(1)–C(4)	1.420(14)
S(1)–C(1)	1.733(9)	C(2)–C(3)	1.523(13)
S(2)–C(1)	1.732(9)	C(4)–C(5)	1.530(14)
N(1)–C(1)	1.304(11)	Zn(1A)–Cl(1A)	2.235(7)
N(1)–C(2)	1.462(12)	Zn(1B)–Cl(1B)	2.294(11)
Angle	ω, deg	Angle	ω, deg
S(1)Au(1)S(2)	75.36(8)	Cl(1A)Zn(1A)Cl(1A)[d]	107.6(4)
S(1)Au(1)S(2)[a]	104.64(8)		
Au(1)S(1)C(1)	86.8(3)	Cl(1A)Zn(1A)Cl(1A)[e]	110.4(2)
Au(1)S(2)C(1)	86.7(3)	Cl(1B)Zn(1B)Cl(1B)[d]	101.4(9)
S(1)C(1)S(2)	111.2(5)	Cl(1B)Zn(1B)Cl(1B)[f]	113.6(5)
Angle	φ, deg	Angle	φ, deg
Au(1)S(1)S(2)C(1)	–177.5(5)	S(1)C(1)N(1)C(5)	–176.8(7)
S(1)Au(1)C(1)S(2)	–177.8(5)	S(2)C(1)N(1)C(2)	179.2(7)
S(1)C(1)N(1)C(2)	1(1)	S(2)C(1)N(1)C(5)	2(1)
Compound **II**			
Bond	*d*, Å	Bond	*d*, Å
Cation A			
Au(1)–S(11)	2.337(2)	N(1)–C(2)	1.465(10)
Au(1)–S(12)	2.332(2)	N(1)–C(5)	1.466(10)
Au(1)···S(21)	3.627(2)	O(1)–C(3)	1.406(10)
S(11)–C(1)	1.729(8)	O(1)–C(4)	1.438(11)
S(12)–C(1)	1.730(9)	C(2)–C(3)	1.539(11)
N(1)–C(1)	1.324(10)	C(4)–C(5)	1.519(13)
Cation B			
Au(2)–S(21)	2.330(2)	N(2)–C(10)	1.478(10)
Au(2)–S(22)	2.337(2)	N(3)–C(11)	1.281(10)
Au(2)–S(23)	2.340(2)	N(3)–C(12)	1.467(11)
Au(2)–S(24)	2.321(2)	N(3)–C(15)	1.483(11)
Au(2)···S(12)[a]	3.665(2)	O(2)–C(8)	1.441(11)
Au(2)···S(32)	3.701(2)	O(2)–C(9)	1.413(11)
S(21)–C(6)	1.716(9)	O(3)–C(13)	1.435(12)
S(22)–C(6)	1.744(9)	O(3)–C(14)	1.433(12)
S(23)–C(11)	1.731(9)	C(7)–C(8)	1.498(13)
S(24)–C(11)	1.750(8)	C(9)–C(10)	1.521(12)
N(2)–C(6)	1.300(10)	C(12)–C(13)	1.508(13)
N(2)–C(7)	1.475(11)	C(14)–C(15)	1.502(12)
Cation C			
Au(3)–S(31)	2.338(2)	N(4)–C(17)	1.471(11)
Au(3)–S(32)	2.339(2)	N(4)–C(20)	1.469(11)
Au(3)···S(23)	4.111(2)	O(4)–C(18)	1.433(10)
S(31)–C(16)	1.733(8)	O(4)–C(19)	1.430(11)
S(32)–C(16)	1.737(8)	C(17)–C(18)	1.502(12)
N(4)–C(16)	1.300(10)	C(19)–C(20)	1.501(12)

Table 2. (Contd.)

Angle	ω, deg	Angle	ω, deg
	Cation A		
S(11)Au(1)S(12)	75.58(8)	Au(1)S(12)C(1)	86.4(3)
Au(1)S(11)C(1)	86.3(3)	S(11)C(1)S(12)	111.6(5)
	Cation B		
S(21)Au(2)S(22)	75.77(8)	Au(2)S(21)C(6)	86.6(3)
S(21)Au(2)S(23)	179.08(8)	Au(2)S(22)C(6)	85.7(3)
S(21)Au(2)S(24)	103.50(8)	Au(2)S(23)C(11)	86.7(3)
S(22)Au(2)S(23)	105.12(8)	Au(2)S(24)C(11)	86.9(3)
S(22)Au(2)S(24)	176.92(8)	S(21)C(6)S(22)	111.9(5)
S(23)Au(2)S(24)	75.62(8)	S(23)C(11)S(24)	110.3(4)
	Cation C		
S(31)Au(3)S(32) S(31)Au(3)S(32)[b]	75.30(7) 104.70(7)	Au(3)S(32)C(16)	86.8(3)
Au(3)S(31)C(16)	87.0(3)	S(31)C(16)S(32)	110.8(5)
Angle	φ, deg	Angle	φ, deg
	Cation A		
Au(1)S(11)S(12)C(1)	−177.6(5)	S(11)C(1)N(1)C(5)	177.3(7)
S(11)Au(1)C(1)S(12)	−177.0(5)	S(12)C(1)N(1)C(2)	−172.2(6)
S(11)C(1)N(1)C(2)	7(1)	S(12)C(1)N(1)C(5)	−2(1)
	Cation B		
Au(2)S(21)S(22)C(6)	−177.2(5)	S(22)C(6)N(2)C(7)	−178.3(6)
Au(2)S(23)S(24)C(11)	172.9(5)	S(22)C(6)N(2)C(10)	−5(1)
S(21)Au(2)C(6)S(22)	177.5(5)	S(23)C(11)N(3)C(12)	2(1)
S(23)Au(2)C(11)S(24)	173.6(5)	S(23)C(11)N(3)C(15)	−168.5(7)
S(21)C(6)N(2)C(7)	−1(1)	S(24)C(11)N(3)C(12)	−179.8(7)
S(21)C(6)N(2)C(10)	172.0(6)	S(24)C(11)N(3)C(15)	9(1)
	Cation C		
Au(3)S(31)S(32)C(16)	177.0(5)	S(31)C(16)N(4)C(20)	178.9(7)
S(31)Au(3)C(16)S(32)	177.3(5)	S(32)C(16)N(4)C(17)	−178.9(6)
S(31)C(16)N(4)C(17)	2(1)	S(32)C(16)N(4)C(20)	−2(1)

* Symmetry codes: [a] $1/2 - x, 1/2 - y, 1/2 - z$; [b] $x, y, z - 1$; [d] $-x, 1/2 - y, z$; [e] $1/4 - x, y - 1/4, 5/4 - z$; [f] $1/4 - x, y - 1/4, 1/4 - z$ (**I**); [a] $-x, -y, -z$; [b] $1 - x, 1 - y, 1 - z$ (**II**).

organization of the new compound **II** formed in the $[Zn_2\{S_2CN(CH_2)_4O\}_4]$–$[AuCl_4]^-$/2M HCl system. To verify these conclusions, the molecular and supramolecular structures of the obtained complexes were solved by single-crystal X-ray diffraction.

The unit cells of the compounds **I** and **II** include four ($[Au\{S_2CN(CH_2)_4O\}_2]_2[ZnCl_4] \cdot 2H_2O$) and eight ($[Au\{S_2CN(CH_2)_4O\}_2]Cl \cdot 2H_2O$) formula units, respectively (Figs. 2 and 3). In both cases, the cationic moiety is represented by the $[Au\{S_2CN(CH_2)_4O\}_2]^+$ complex ions in which the central gold atom coordinates two MfDtc ligands in the S,S'-bidentate mode (Figs. 4 and 5). The structurally equivalent MfDtc ligands in compound **I** have a nearly isobidentate coordination: the Au–S bond lengths differ little (2.336 and 2.340 Å). The structure of complex **II** includes three non-equivalent complex cations: A with the Au(1) atom, B (Au(2)), and C (Au(3)) (Fig. 5). In the centrosymmetrical cations A and C, the ligands are also coordinated in the isobidentate mode by the central gold atom: the Au–S bond lengths are 2.332 and 2.337 Å (A); 2.338 and 2.339 Å (C). One of the structurally non-equivalent ligands in cation B is reliably S,S'-anisobidentate, although the Au–S

Table 3. Geometric parameters of hydrogen bonds in complex **II***

D–H···A contact	Distance, Å		DHA angle, deg
	D···A	H···A	
O(1*w*)–H(1*wA*)···Cl(1)	3.143(8)	2.33(5)	157(10)
O(1*w*)–H(1*wB*)···Cl(1)[a]	3.193(9)	2.32(4)	165(11)
O(2*w*)–H(2*wA*)···Cl(1)	3.338(9)	2.54(6)	148(10)
O(2*w*)–H(2*wB*)···Cl(2)	3.219(9)	2.34(4)	166(12)
O(3*w*)–H(3*wA*)···Cl(1)	3.122(10)	2.57(8)	120(7)
O(3*w*)–H(3*wB*)···Cl(2)	3.128(10)	2.26(4)	163(11)
O(4*w*)–H(4*wA*)···Cl(2)	3.164(9)	2.32(6)	158(13)
O(4*w*)–H(4*wB*)···Cl(2)[b]	3.215(10)	2.42(6)	148(10)

* Symmetry codes: [a] $-x, 1-y, -z$; [b] $1-x, 1-y, 1-z$.

bond lengths are not very different (2.321 and 2.340 Å). Thus, as was to be expected from the ^{13}C MAS NMR data, the structure of compound **II** comprises four non-equivalent Dtc ligands.

In each cation, this mode of coordination of MfDtc is accompanied by the formation of two four-membered [AuS_2C] metal rings sharing the gold atom. In these rings of **I**/**II**, the Au···C (2.828/2.810–2.835 Å) and S···S (2.858/2.857–2.866 Å) interatomic distances, which are much shorter than the sums of the van der Waals radii of the corresponding pairs of atoms: 3.36 Å and 3.60 Å [21, 22], reflect their small size with substantially proximate positions of gold and carbon atoms. The latter fact may be attributed to the direct transannular interaction between these atoms and reflect high π-electron density inside the rings. In the [AuS_2C] groups, the atoms show some tetrahedral deviation from the plane: the AuSSC torsion angles are 172.88°–177.50° and the SAuCS torsion angles are 173.58°–177.76°. This distortion can be represented as folding of the [AuS_2C] metal rings along the S–S axis: the dihedral angle between the [AuSS] and [SSC] half-ring planes is 177.50° in **I** and 176.62°, 176.97°, 172.88°, and 177.18° in **II**. The geometry of the [AuS_4] chromophores is nearly planar-tetragonal, which implies a low-spin (intraorbital) dsp^2 hybrid state of gold(III) with C.N. 4. In the MfDtc ligands, the $C_2NC(S)S$ groups are almost coplanar: the SCNC torsion angles are close to 180° or 0° (significant deviations are found only for C(6) and C(11) in cation B of compound **II**). This fact and also the higher strength of the N–C(S)S bonds compared with the N–CH_2 bonds (Table 2) are due to the mesomeric effect of the dithiocarbamate groups. The morpholine heterocycles in all MfDtc ligands exist in the chair conformation: the angles inside the rings are 112.96°–109.36° (admixture of the sp^2 hybrid state for nitrogen atoms results in increase in the CNC angles to 113.36°–115.69°), and the bond lengths are as follows: C–O, 1.406–1.441 Å; C–N, 1.462–1.483 Å. The peripheral morpholine heterocycles demonstrate the opposite spatial direction relative to the plane of the [AuS_4] chromophores (*trans*-orientation).

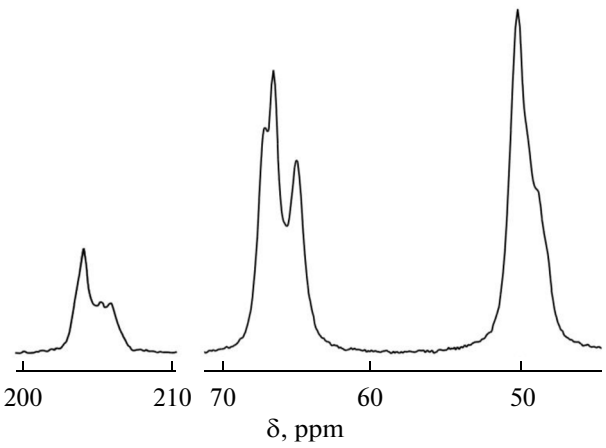

Fig. 1. MAS ^{13}C NMR spectrum of complex **II** (number of transients/spinning frequency of 13000/5100 Hz).

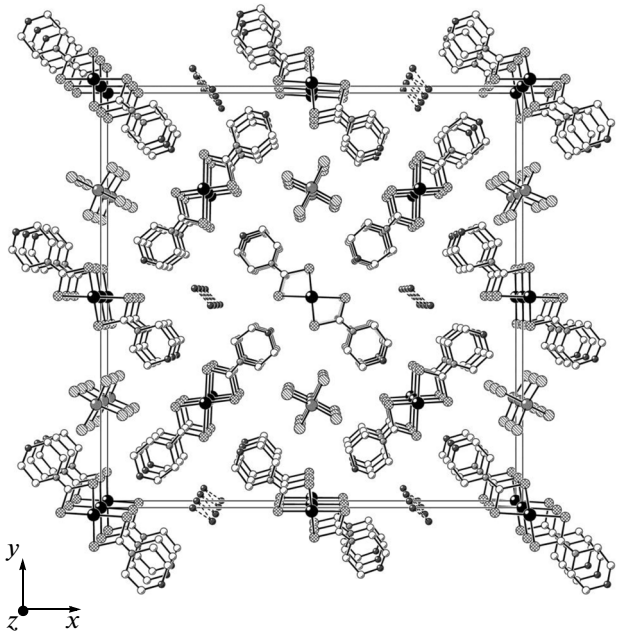

Fig. 2. Unit cell of **I** projected on *xy* plane.

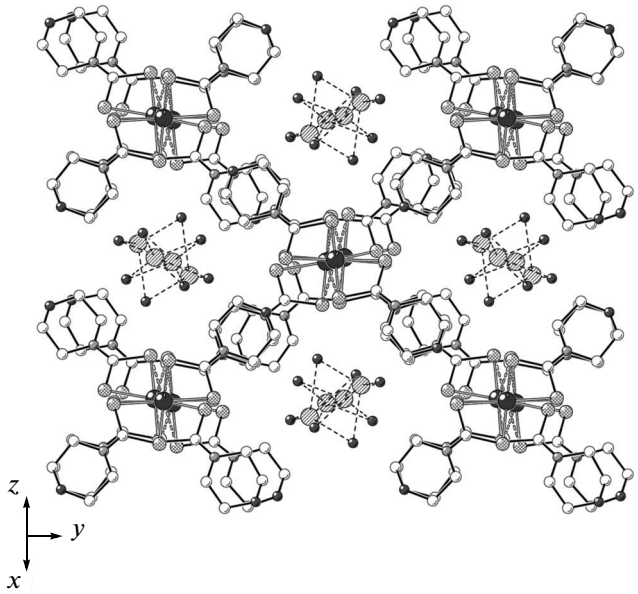

Fig. 3. Unit cell **II** projected on *xz* plane.

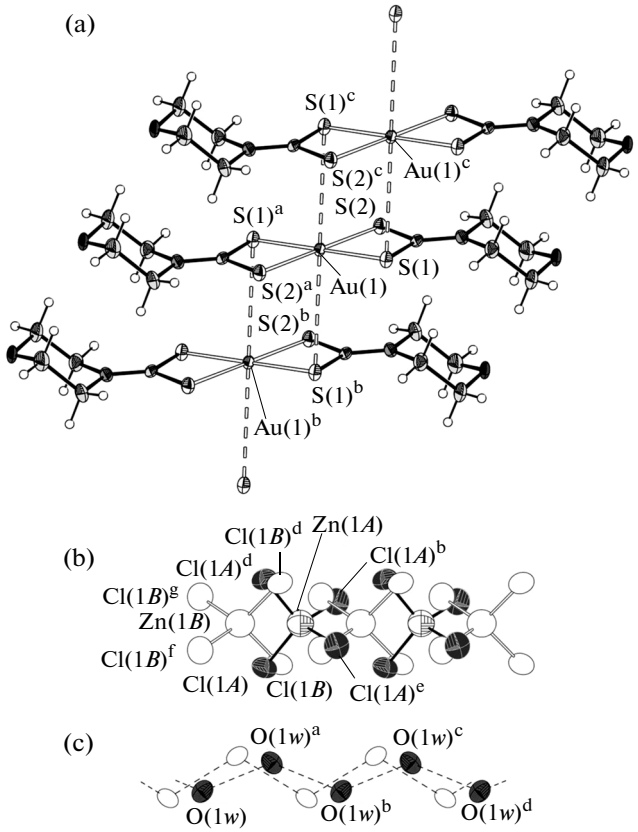

Fig. 4. (a) Structural fragment of the cationic polymeric chain of complex **I**, the secondary Au···S bonds are shown by dashed lines; 50% probability ellipsoids; (b) schematic view of the structurally disordered $[ZnCl_4]^{2-}$ anions: A (50% probability ellipsoids, 0.8 occupancy of atomic sites) and B (0.2 occupancy); (c) chain fragments composed of disordered H_2O molecules with 0.5 site occupancy (the hydrogen bonds are shown by dashed lines; symmetry codes: (a) $1/2 - x, -y, 1/2 + z$; (b) $x, y, 1 + z$; (c) $1/2 - x, -y, 3/2 + z$; (d) $x, y, 2 + z$).

The anionic moiety of the complexes is formed by the distorted tetrahedral $[ZnCl_4]^{2-}$ ion (**I**) (Fig. 4b) or Cl^- ion (**II**) (Fig. 5b). The $[ZnCl_4]^{2-}$ anions are statistically disordered between two positions A and B in 0.8 : 0.2 ratio. The central zinc atom occurs in the sp^3-hybridized state: the ClZnCl angles in A are close to the purely tetrahedral value, while in B, they considerably differ from the tetrahedral angle (Table 2). The Cl atoms in anion A, and also in B are structurally equivalent; however, the Zn(A)–Cl(A) bonds (2.235 Å) are somewhat shorter than Zn(B)–Cl(B) (2.294 Å) (Table 2). However, in both cases, the Zn–Cl bond length is consistent with reported data [23, 24].

The further structural ordering of **I** and **II** at the supramolecular level is due to relatively weak Au···S non-valence secondary interactions.[1] In complex **I** the Au(1) atom of each $[Au\{S_2CN(CH_2)_4O\}_2]^+$ cation forms two secondary bonds with MfDtc sulfur atoms of two neighboring cations: Au(1)···S(1)^b and Au(1)···S(1)^c of 3.663 Å (the sum of the van der Waals radii of the gold and sulfur atoms is 3.46 Å [21, 22]). This gives the linear chains $([Au\{S_2CN(CH_2)_4O\}_2]^+)_n$ directed along the crystallographic *z* axis (the Au···Au distance is 4.421 Å and the AuAuAu angle is 180°). The stacks of the $[ZnCl_4]^{2-}$ complex anions and zigzag-like chains of water molecules combined by hydrogen bonds are located between the cationic chains (Figs. 2, 4a).

[1] The concept of secondary bonds was first proposed in [25] to describe the contacts that occur at distances comparable with the sums of the van der Waals radii of the corresponding atoms.

In compound **II**, the polymer chains comprise three structurally non-equivalent complex cations. In non-centrosymmetric cation B, two diagonally arranged sulfur atoms of structurally non-equivalent =NC(S)S– groups are involved in non-valence contacts with the Au(1) and Au(3) atoms of neighboring centrosymmetric cations A and C: the S(21)···Au(1) distance is 3.627 Å and the S(23)···Au(3) distance is 4.111 Å. In turn, the Au(2) atom forms additional strong bonds, Au(2)···S(12)^a 3.665 Å and Au(2)···S(32) 3.701 Å (Table 2, Fig. 5a), which enhances the overall binding strength between isomeric complex cations. The formation of these Au···S secondary bonds gives rise to chains with non-equivalent complex cations $[\cdots B\cdots A\cdots B\cdots C\cdots]_n$ alternating along their length with distances: Au(1)···Au(2) 4.384 Å, and Au(2)···Au(3) 4.777 Å; and with the angles: Au(1)Au(2)Au(3),

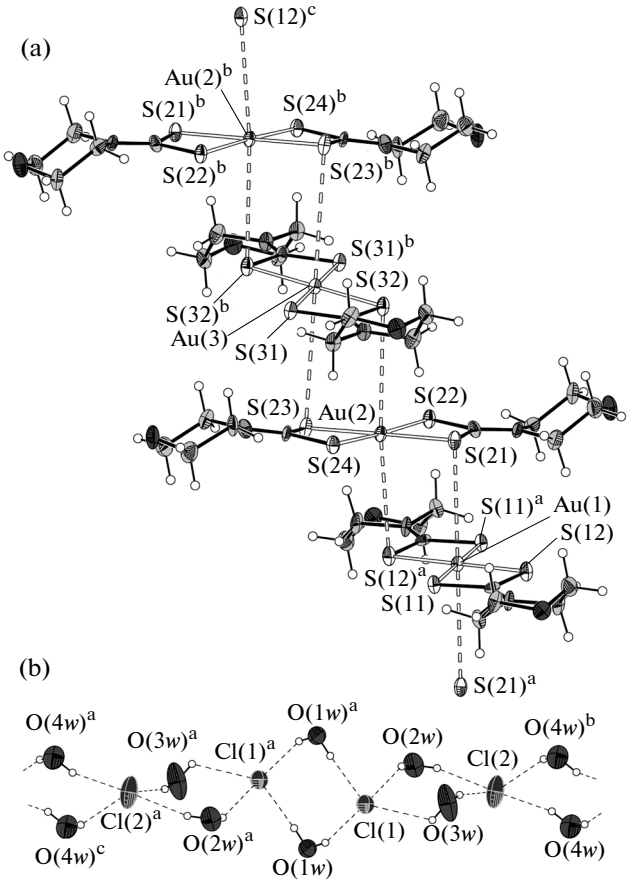

Fig. 5. (a) Structural fragment of the cationic polymeric chain of complex **II**, the secondary Au···S bonds are shown by dashed lines; (b) hydrogen bonds between structurally non-equivalent H_2O molecules and Cl^- ions in complex **II** (dashed lines) (b). 50% probability ellipsoids.

169.58°; Au(2)Au(1)Au(2), 180°; and Au(2)Au(3)Au(2), 180°. The neighboring cations in the chain are oriented in such a way that their bisecting axes (passing through the bicyclic $[CS_2AuS_2C]$ moiety) are mutually perpendicular, while the closest centrosymmetrical cations B are, in addition, antiparallel (Figs. 3 and 5a).

The structure of **II** comprises four non-equivalent H_2O molecules and two Cl^- anions, which also participate in the construction of polymeric chains through hydrogen bonding (the mode of chain construction is shown in Fig. 5b). The non-equivalence of Cl^- ions and water molecules is illustrated by differences between the geometric parameters of the formed hydrogen bonds (Table 3). These chains are located in through cavities (like channels), which are separated in space by zigzag-like cation chains (Fig. 3).

The thermal behavior of **I** and **II** was studied by STA. The TG curve (Figs. 6a and 7a) of each compound comprises three mass loss stages: (1) dehydration of complexes (~70–200°C), (2) thermal destruction of their dehydrated forms (~200–350°C), and (3) desorption and evaporation of the thermolysis products (~350–850°C). In the initial stage of TG curves of **I**/**II**, the mass loss is 2.08/6.00%, which is close to the theoretically calculated values (2.80/6.08%) for two solvating water molecules. The steeply descending segments of the next stage show the major mass loss (51.83/48.83%) related to the intense thermolysis of dehydrated complexes. The thermal destruction of **II** is accompanied by reduction of gold(III) to the metal-

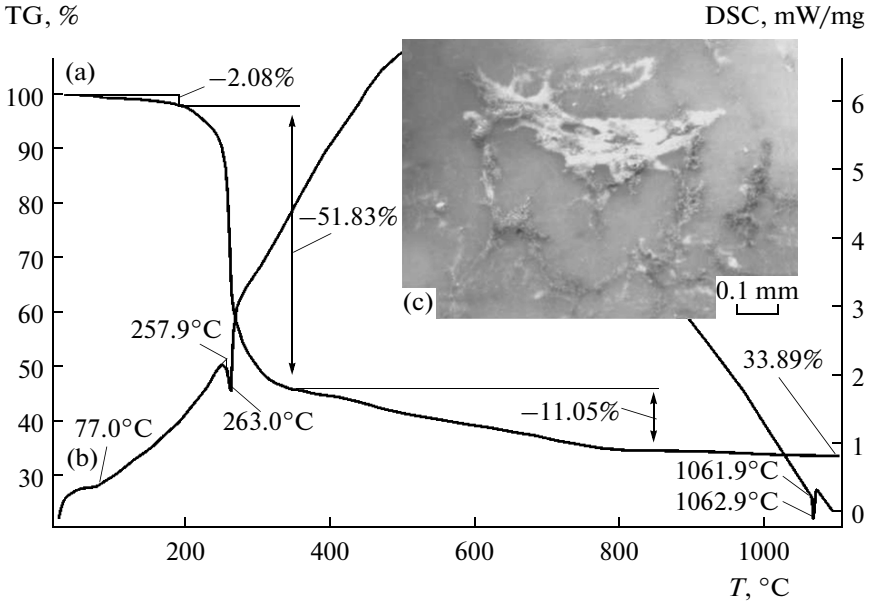

Fig. 6. (a) TG and (b) DSC curves for complex **I**. (c) Enlarged fragment of the crucible bottom after the m.p. has been passed.

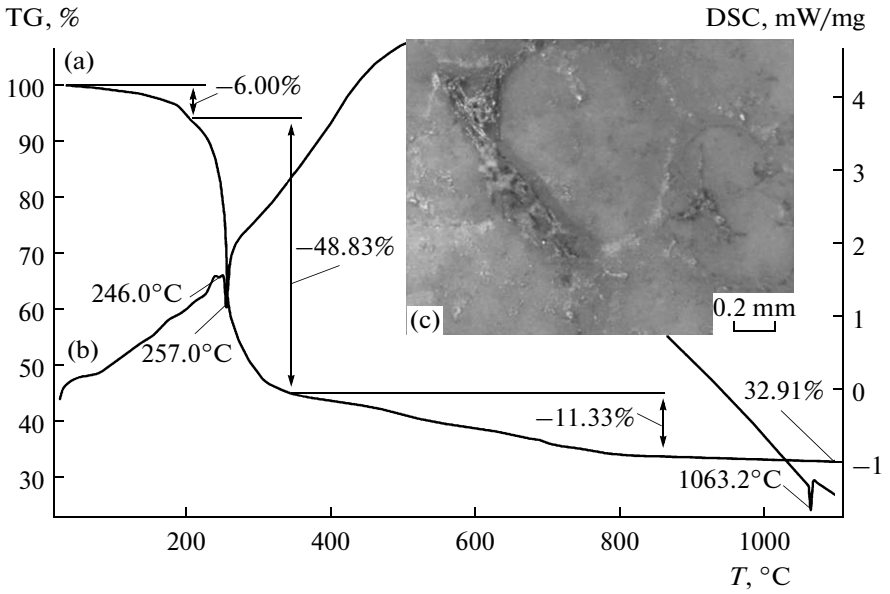

Fig. 7. (a) TG and (b) DSC curves for complex **II**. (c) Enlarged fragment of the crucible bottom after the m.p. has been passed.

lic state. In the case of complex **I**, in addition to gold(III) reduction in the cation, release of $ZnCl_2$ and its partial transformation into ZnS (in the anion) was noted.[2] For this stage of thermolysis of **I**/**II**, the corresponding segments of the DSC curves (Figs. 6b and 7b) record endotherms with extrema at 263.0/257.0°C. In the case of **II**, this endotherm is preceded by a less intense peak referred to melting of the complex (extrapolated m.p. = 242.4°C). An independent determination of the melting point in a glass capillary showed melting at 236°C.

The last stage reflects smooth desorption and evaporation of the products of thermolysis of **I**/**II** (11.05/11.33%) including evaporation of $ZnCl_2$ in the case of **I** (m.p. = 317°C and b.p. = 733°C [27]). The final thermolysis product is the reduced metallic gold: the DSC curves show the endotherms corresponding to melting (extrapolated m.p. = 1061.9/1061.4°C). The residual mass of complex **II** at 1100°C (32.91% of the initial mass) does not differ much from the calculated value (33.22%) for the reduced gold, which was identified as the only final product of thermal transformations of **II** (Fig. 7c). The residual mass formed from complex **I** at 1100°C (33.89%) markedly exceeds the value expected for reduced gold (calcd. 30.63%). The excess mass (3.26%) should be attributed to ZnS (sublimes at 1185°C [23]), the formation of which requires 43% of the amount of zinc contained in the complex. Thus, 57% of zinc remains as $ZnCl_2$, the desorption of which together with other volatile products is reflected in the last segment of the TG curve. After opening of the crucible, associates of tiny beads of reduced gold with white bloom of zinc sulfide were detected on the surface (Fig. 6c).

[2] In [26], the formation of metal sulfides upon the thermolysis of complexes containing sulfur ligands is substantiated by thermodynamic reasons.

ACKNOWLEDGMENTS

The authors are grateful to Professor O.N. Antzutkin (Luleå University of Technology, Sweden) for providing the possibility to record the MAS ^{13}C NMR spectra.

This work was partially supported by the Fundamental Research Program of the Presidium of the RAS "Development of the Methods for the Synthesis of Chemical Compounds and for the Design of Novel Materials" and the Presidium of the Far East Branch of the RAS (projects no. 12-I-P8-01 and 12-III-A-04-040).

REFERENCES

1. Hogarth, G., *Prog. Inorg. Chem.,* 2005, vol. 53, p. 71.
2. Zemskova, S.M., Glinskaya, L.A., Klevtsova, R.F., and Larionov, S.V., *Zh. Neorg. Khim.*, 1993, vol. 38, no. 3, p. 466.
3. Onwudiwe, D.C. and Ajibade, P.A., *Mater. Lett.*, 2011, vol. 65, nos. 21–22, p. 3258.
4. Saravanan, M., Ramalingam, K., Bocelli, G., and Olla, R., *Appl. Organomet. Chem.*, 2004, vol. 18, no. 2, p. 103.
5. Onwudiwe, D.C., Strydom, C., Oluwafemi, O.S., and Songca, S.P., *Mater. Res. Bull.*, 2012, vol. 47, no. 12, p. 4445.
6. Srinivasan, N. and Thirumaran, S., *Superlatt. Microstruct.*, 2012, vol. 51, no. 6, p. 912.

7. Botelho, J.R., Souza, A.G., Gondim, A.D., et al., *J. Therm. Anal. Calorim.*, 2005, vol. 79, no. 2, p. 30.
8. Chesman, A.S.R., van Embden, J., Duffy, N.W., et al., *Cryst. Growth Des.*, 2013, vol. 13, p. 1712.
9. Shahid, M., Ruffer, T., Lang, H., et al., *J. Coord. Chem.*, 2009, vol. 62, no. 3, p. 440.
10. Shaheen, F., Gieck, C., Badshah, A., and Khosa, M.K., *Acta Crystallogr., Sect. E: Structure Reports Online*, 2006, vol. 62, no. 6, p. m1186.
11. Loseva, O.V., Rodina, T.A., and Ivanov, A.V., *Russ. J. Coord. Chem.,* 2013, vol. 39, no. 6 p. 463.
12. Ivanov, A.V., Loseva, O.V., Rodina, T.A., et al., *Dokl. Phys. Chem.*, 2013, vol. 452, no. 2, p. 223.
13. Loseva, O.V., Rodina, T.A., Gerasimenko, A.V., and Ivanov, A.V., *Russ. J. Inorg. Chem.*, 2013, vol. 58, no. 9, p. 1104.
14. Rodina, T.A., Loseva, O.V., Ivanov, A.V., et al., *Russ. J. Coord. Chem.*, 2013, vol. 39, no. 10, p. 694.
15. Byr'ko, V.M., *Ditiokarbamaty* (Dithiocarbamates), Moscow: Nauka, 1984.
16. Ivanov, A.V., Ivakhnenko, E.V., Gerasimenko, A.V., and Forsling, V., *Russ. J. Inorg. Chem.*, 2003, vol. 48, no. 1, p. 45.
17. Hexem, J.G., Frey, M.H., and Opella, S.J., *J. Chem. Phys.*, 1982, vol. 77, no. 7, p. 3847.
18. Harris, R.K., Jonsen, P., and Packer, K.J., *Magn. Reson. Chem.*, 1985, vol. 23, no. 7, p. 565.
19. Pines, A., Gibby, M.G., and Waugh, J.S., *J. Chem. Phys.*, 1972, vol. 56, no. 4, p. 1776.
20. *APEX2 (version 1.08), SAINT (version 7.03), SADABS (version 2.11) and SHELXTL (version 6.12)*, Madison (WI, USA): Bruker AXS Inc., 2004.
21. Pauling, L., *The Nature of the Chemical Bond and the Structure of Molecules and Crystals*, London: Cornell Univ. Press, 1960.
22. Bondi, A., *J. Phys. Chem.*, 1964, vol. 68, no. 2, p. 441.
23. Exarchos, G., Robinson, S.D., and Steed, J.W., *Polyhedron*, 2001, vol. 20, nos. 24–25, p. 2951.
24. Karâa, N., Hamdi, B., Ben Salah, A., and Zouari, R., *J. Mol. Struct.*, 2013, vol. 1049, nos. 1–3, p. 48.
25. Alcock, N.W., *Adv. Inorg. Chem. Radiochem.*, 1972, vol. 15, no. 2, p. 1.
26. Razuvaev, G.A., Almazov, G.V., Domrachev, G.A., et al., *Dokl. Akad. Nauk SSSR*, 1987, vol. 294, no. 1, p. 141.
27. Lidin, R.A., Andreeva, L.L., and Molochko, V.A., *Spravochnik po neorganicheskoi khimii* (Handbook in Inorganic Chemistry), Moscow: Khimiya, 1987.

Translated by Z. Svitanko